2001

Static friction and surface roughness studies of surface micromachined electrostatic micromotors using an atomic force/friction force microscope

Sriram Sundararajan, *The Ohio State University*
Bharat Bhushan, *The Ohio State University*

JVSTA Journal of Vacuum Science & Technology A

Static friction and surface roughness studies of surface micromachined electrostatic micromotors using an atomic force/friction force microscope

Sriram Sundararajan and Bharat Bhushan

Citation: Journal of Vacuum Science & Technology A **19**, 1777 (2001); doi: 10.1116/1.1353539
View online: http://dx.doi.org/10.1116/1.1353539
View Table of Contents: http://scitation.aip.org/content/avs/journal/jvsta/19/4?ver=pdfcov
Published by the AVS: Science & Technology of Materials, Interfaces, and Processing

Static friction and surface roughness studies of surface micromachined electrostatic micromotors using an atomic force/friction force microscope

Sriram Sundararajan and Bharat Bhushan[a)]
Computer Microtribology and Contamination Laboratory, The Ohio State University, 206 West 18th Avenue, Columbus, Ohio 43210-1107

(Received 11 September 2000; accepted 15 January 2001)

A technique to measure the static friction forces (stiction) encountered in surface micromachined micromotors using a commercial atomic force microscope (AFM)/friction force microscope has been developed and is described. An AFM tip is pushed against a rotor arm of the micromotor so as to generate lateral deflection (torsion) of the tip, which is measured by the AFM. The maximum value of the lateral deflection obtained prior to rotor movement (rotation) is a measure of the static friction force of the micromotors. This technique was employed to study the effect of humidity and rest time on the static friction force of polysilicon motors, both unlubricated and lubricated using perfluoropolyether lubricants. Surface roughness parameters (rms, peak-to-valley distance, skewness, and kurtosis) and microscale friction properties of the various surfaces of the motor were measured. Dramatic differences between the roughness of the underside and top surfaces of the rotor and between the surface beneath the rotor and adjacent areas were observed. The mechanisms responsible for stiction in such devices are discussed. Lubrication methods to minimize friction problems are also presented. © *2001 American Vacuum Society.* [DOI: 10.1116/1.1353539]

I. INTRODUCTION

Microelectromechanical systems (MEMS) have undergone significant advances over the last two decades with researchers fabricating a variety of miniaturized devices with dimensions ranging from a couple to a few thousand microns.[1,2] In MEMS devices, the various forces associated with the devices scale with the size. As a result, surface forces such as friction, adhesion, meniscus forces, viscous drag and surface tension that are proportional to area, become a thousand times larger than the forces proportional to the volume, such as inertial and electromagnetic forces. Since the start-up forces and torques involved in MEMS operation available to overcome retarding forces are small, the increase in resistive forces such as friction and adhesion become serious tribological concerns that limit the life and reliability of MEMS devices.[3,4] There are also adhesion problems during surface micromachining fabrication processes in which the suspended microstructures can sometimes collapse and permanently adhere to the underlying substrate. In addition to the consequence of a large surface-to-volume ratio, since MEMS devices are designed for small tolerances, physical contact becomes more likely, which makes them particularly vulnerable to adhesion between adjacent components. A large lateral force required to initiate relative motion between two smooth surfaces is referred to as ''stiction,'' which has been studied extensively in tribology of magnetic storage systems.[5] Limited studies have also been conducted to address stiction issues in surface micromachining of MEMS.[3,6–9] In MEMS devices involving parts in relative motion to each other, such as micromotors, large friction forces become the limiting factor to the successful operation and reliability of the device. It is generally known that most micromotors cannot be rotated as manufactured and require some form of lubrication. It is therefore critical to determine the friction forces present in such MEMS devices. Table I presents static friction coefficients of various MEMS devices evaluated by various researchers.[10–13] Most of these techniques employ indirect methods to determine the friction forces or involve fabrication of complex structures. A direct method to measure friction forces in MEMS is needed. The effects of environmental conditions on these forces must also be understood. Effective lubrication methods for these devices need to be determined.

The advent of atomic force/friction force microscopy has resulted in extensive studies of surface topography, adhesion, friction, wear, lubrication, and several other surface phenomena on a micro/nanoscale.[14] The atomic force/friction force microscope (AFM/FFM) is an ideal instrument for direct measurements of surface phenomena on MEMS devices, components, and their surfaces. In this paper, we present a novel technique to measure the static friction force (stiction) encountered in surface micromachined polysilicon electrostatic micromotors using an AFM. Self-assembled monolayers have been explored for lubrication of MEMS.[15–17] In this study, the use of perfluoropolyether (PFPE) liquid lubricants to reduce friction/stiction for micromotors is investigated and the effect of humidity on the friction forces of unlubricated and lubricated devices is studied as well. Mechanisms for the observed friction phenomena are discussed. For the first time, surface roughness of micromotor components is measured and the effect of fabrication steps on surface roughness is discussed.

a)Electronic mail: bhushan.2@osu.edu

TABLE I. Published data on coefficient of static friction measurements of MEMS devices and structures.

Reference	Test method	Device/structure	Material pairs	Environment	Coefficient of static friction
10	Starting voltage	IC-processed micromotor	PolySi/Si_3N_4	Air	0.20–0.40
11	Electrostatic	Comb-drive	PolySi/PolySi	Air	4.9 ± 1.0
	loading	microstructure	PolySi/Si_3N_4		2.5 ± 0.5
12	Pull-off force	Silicon microbeams	SiO_2/SiO_2	Air	2.1 ± 0.8
13	Cantilever/fiber deflection rig	LIGA micromotors	Ni/alumina	Air	0.6–1.2

II. POLYSILICON MICROMOTORS

A. Polysilicon electrostatic micromotors

Figure 1 shows an optical micrograph of the polysilicon electrostatic micromotors used in this study. These motors were fabricated via surface micromachining.[2] Surface micromachining, defined as the fabrication of microstructures from deposited thin films, involves deposition and etching sacrificial thin films to produce a free-standing structure. Figure 2(a) describes the various steps involved in the surface micromachining of the micromotors used in this study. The first step involves deposition of isolation layers that isolate the micromotor components electrically up to 300 V and avoid mechanical deformation of the substrate. These consist of a 600-nm-thick layer of thermal oxide (produced at 1100 °C in oxygen atmosphere for 1–2 h) followed by a 500-nm-thick silicon nitride layer deposited by low-pressure chemical vapor deposition (LPCVD). A 2-μm-thick polysilicon layer is then deposited at 605 °C by LPCVD followed by deposition of thermal oxide, which forms the first sacrificial layer. A second polysilicon layer is then deposited, which is subsequently patterned and vertically etched by SF_6 plasma etching to form the rotor and stator electrodes. The first sacrificial layer is then opened up by isotropic wet chemical etching with buffer HF down to the polysilicon layer in the center of the micromotor where the motor hub will be deposited. This geometry allows the rotor to be supported near the hub axis in an attempt to reduce the friction torque. Conductivity of the polysilicon rotor and stator electrodes is then achieved by thermal diffusion of $POCl_3$ at 1050 °C. The second sacrificial layer is deposited at 1000 °C in the presence of steam for 45 min. The advantage of the oxidation is twofold;[18] first, the sacrificial layer conforms to the shape of the rotor and second; the thickness of the layer can be effectively controlled and minimized (420 nm). The motor hub is then deposited at the center (polysilicon). The last step involves the release of the micromotor by selective wet chemical etching of the sacrificial layer by HF (50%). In this study, motors from two batches (M1–M4 and M6–M8 from one batch and M5 from another batch) were used. The difference between the two batches was that the first sacrificial layer was deposited by different deposition systems.

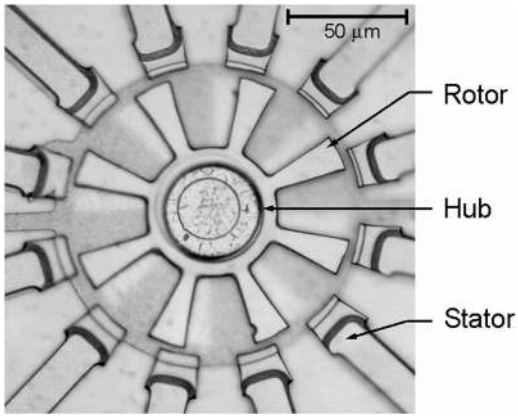

FIG. 1. Optical micrograph of a surface micromachined polysilicon micromotor.

Figure 2(b) shows typical dimensions of a micromotor. Constant contact occurs between the bottom of the rotor and the hub flange while intermittent contact may occur between the rotor and the stator and the rotor and hub circumference during motor operation.

B. Lubrication

Lubrication of a wafer of unlubricated motors with perfluoropolyether lubricant (Z-DOL) was accomplished via a dip-coating technique.[5,19] The sample was vertically submerged in a bath containing a dilute solution of 0.2% Z-DOL lubricant in hydrocarbon solvent (HT-70) for 10 min. The sample was then vertically pulled up from the solution at constant speed and allowed to dry naturally. This resulted in a lubricated sample with a 2-nm-thick coating of as-is Z-DOL. In order to obtain a bonded layer of lubricant (termed Z-DOL BW), the lubricated sample was then baked at 150 °C for 1 h and allowed to cool naturally. Finally, the unbonded portions of the lubricant were removed by dipping the sample in perfluorocarbon liquid (FC-72) for 5 min. This resulted in a bonded film thickness of about 1 nm.

III. EXPERIMENT

A. Atomic force/friction force microscope

A Dimension 3000 AFM (Nanoscope IIIa, Digital Instruments, Santa Barbara, CA) was used in this study. The AFM is equipped with a high magnification video camera and a motorized stage, which facilitate easy location of the area of interest on a micromotor wafer. Topography measurements were made in tapping mode using a standard silicon probe (tip radius of about 10 nm). Microscale friction measurements were conducted using a Si_3N_4 probe (tip radius of about 50 nm, V-shaped cantilever with normal stiffness of 0.6 N/m). For measurement of the static friction forces of the

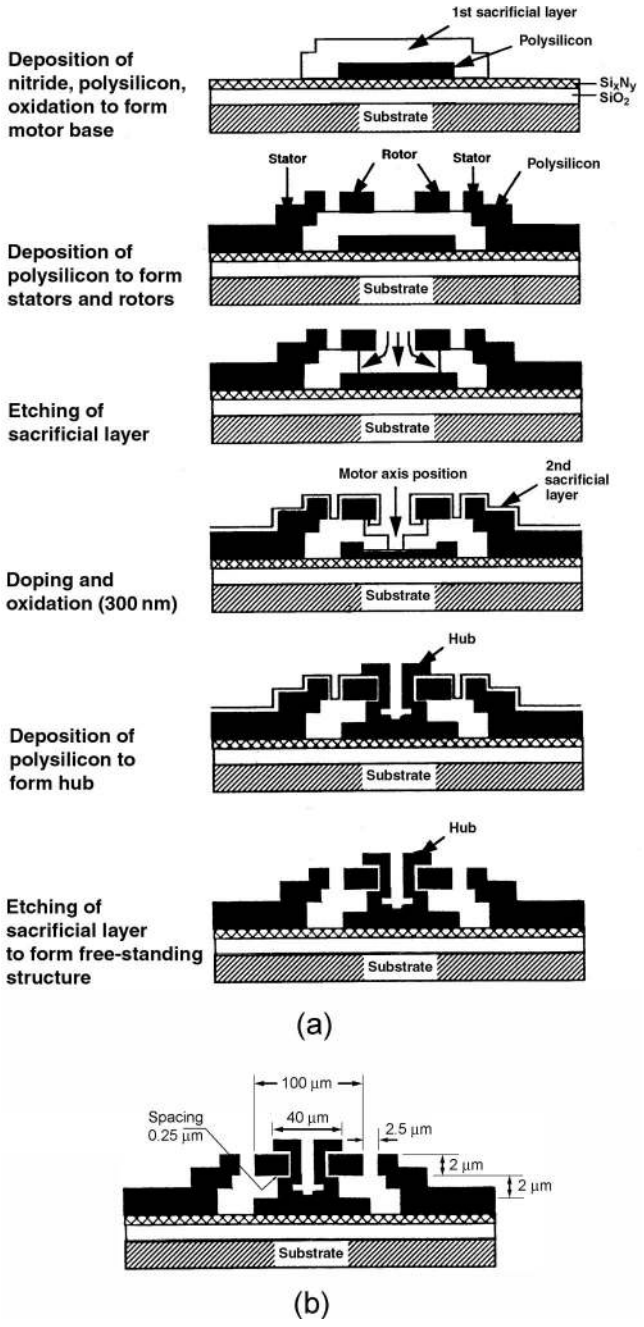

FIG. 2. (a) Fabrication process sequence of surface micromachined polysilicon micromotors. (b) Dimensions of the micromotor; the clearance between the rotor and the hub is about 250 nm. The figures are not to scale.

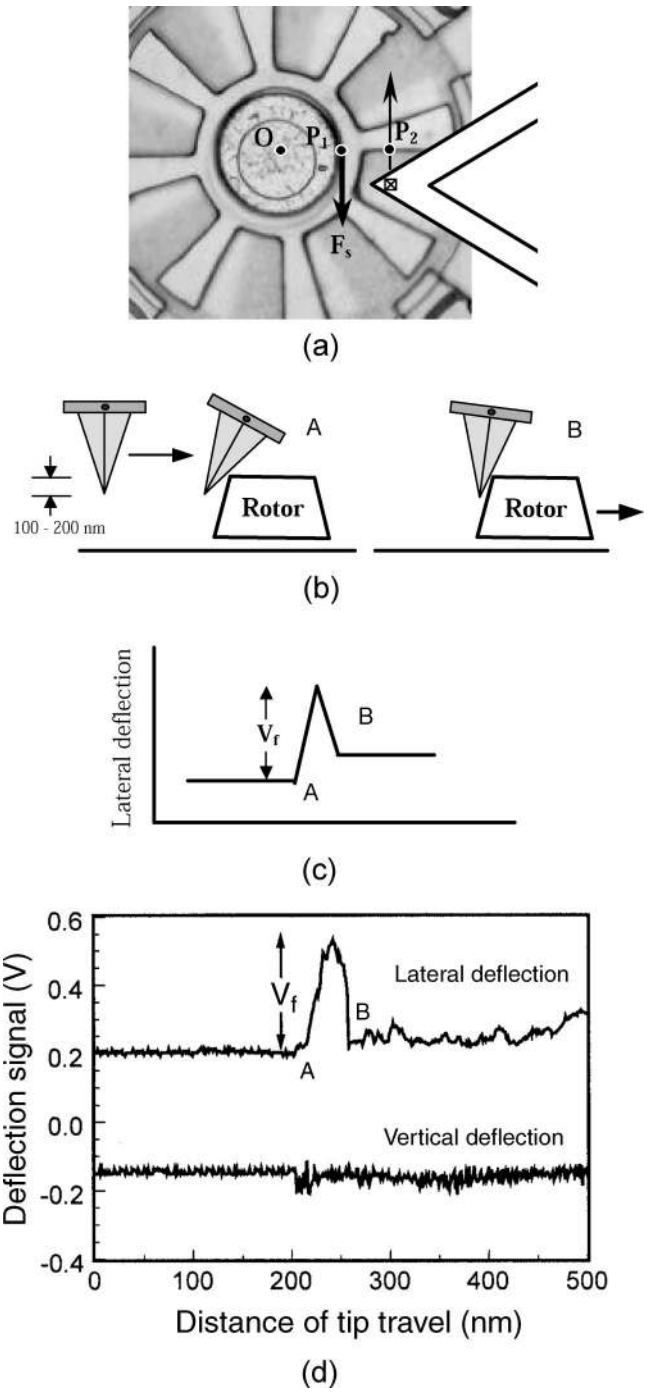

FIG. 3. (a) Schematic of the technique used to measure the force, F_s, required to initiate rotor movement using an AFM/FFM. (b) As the tip is pushed against the rotor, the lateral deflection experienced by the rotor due to the twisting of the tip prior to rotor movement is a measure of static friction force, F_s, of the rotors. (c) Schematic of lateral deflection expected from the above-mentioned experiment. The peak V_f is related to the static friction of the motor. (d) Raw lateral deflection and normal deflection data obtained using an AFM (Si_3N_4 tip) against a rotor.

micromotors, a similar Si_3N_4 probe of lower normal stiffness (0.38 N/m) was used for higher lateral deflection sensitivity.

B. Technique to measure static friction force of the micromotor

Continuous physical contact occurs during rotor movement (rotation) in the micromotors between the rotor and lower hub flange. In addition, contact occurs at other locations between the rotor and the hub surface and between the rotor and the stator. Friction forces will be present at these contact regions during motor operation. Although the actual distribution of these forces is not known, they can be expected to be concentrated near the hub where there is continuous contact. If we therefore represent the static friction force of the micromotor as a single force F_s acting at point P_1 [as shown in Fig. 3(a)], then the magnitude of the fric-

tional torque about the center of the motor (O) that must be overcome before rotor movement can be initiated is

$$T_s = F_s l_1, \tag{1}$$

where l_1 is the distance OP_1, which is assumed to be the average distance from the center at which the friction force F_s occurs. Now consider an AFM tip moving against a rotor arm in a direction perpendicular to the long axis of the cantilever beam (the rotor arm edge closest to the tip is parallel to the long axis of the cantilever beam), as shown in Fig. 3(a). When the tip encounters the rotor at point P_2, the tip will twist generating a lateral force between the tip and the rotor [event A in Fig. 3(b)]. This reaction force will generate a torque about the center of the motor. Since the tip is trying to move further in the direction shown, the tip will continue to twist to a maximum value at which the lateral force between the tip and the rotor becomes high enough such that the resultant torque T_f about the center of the motor equals the static friction torque T_s. At this point, the rotor will begin to rotate and the twist of the cantilever decreases sharply [event B in Fig. 3(b)]. The twist of the cantilever is measured in the AFM as a change in the lateral deflection signal (in volts), which is the underlying concept of friction force microscopy[14] (FFM). The change in the lateral deflection signal corresponding to the above-mentioned events as the tip approaches the rotor is shown schematically in Fig. 3(c). The value of the peak V_f is a measure of the force exerted on the rotor by the tip just before the static frictional torque is matched and the rotor begins to rotate.

The controlled tip movements necessary for this experiment are achieved using the lithography software module (Nanoscript™) of the Nanoscope. This allows the user to write macros to control the movement of the tip with respect to the sample.[20] In this case, the tip is first made to lift off the polysilicon base so as to obtain a 100–200 nm height difference between the rotor top surface and the end of the tip. This is to ensure that the contact point between the tip and the rotor occurs as close to the end of the tip as possible. A single scan or pass is then made at a low speed of 100 nm/s toward the rotor for a fixed distance. During the execution of the lithography module, the regular user interface of the Nanoscope is disabled. Hence the lateral and normal deflection signals are measured via a breakout box and data acquisition computer equipped with a 12 bit analog-to-digital board.

Figure 3(d) shows typical lateral deflection and normal deflection data during an experimental run against a rotor. The lateral deflection signal shows the peak V_f associated with the lateral force required to generate rotor movement (F_f). The rotor movement [rotation about the center point O in Fig. 3(a)] can be visually verified during the experiment via the AFM video camera. The normal deflection signal does not change appreciably during this event, indicating that the tip undergoes twisting similar to the torsion encountered in a regular friction experiment using an AFM.

Equating the torques at this instance about the center of the motor gives an expression to determine the static friction force of the micromotor, F_s:

$$F_s = F_f \frac{l_2}{l_1}, \tag{2}$$

where l_2 is the torque arm of the lateral force about the center of the motor [distance OP_2 in Fig. 3(a)].

To convert the lateral deflection signal V_f to friction force (F_f) a number of calibration experiments are performed. Based on Ruan and Bhushan's method,[21] the AFM tip is traced and retraced across the surface (in contact mode with the slow scan axis disabled) in a direction parallel to the long axis of the cantilever over a range of normal loads. The plot of profile separation (''Trace–Retrace'' value at each location of the scan, directly measured on the AFM) versus average piezo center position results in a linear fit as shown in Fig. 4(a) with a slope (δ) that is related to the coefficient of friction between the tip and sample by [14]

$$\mu = \delta(L/2h), \tag{3}$$

where μ is the coefficient of friction, h is the distance from the end of the tip to the height of the cantilever base, and L is the cantilever length. It is assumed that the normal loads

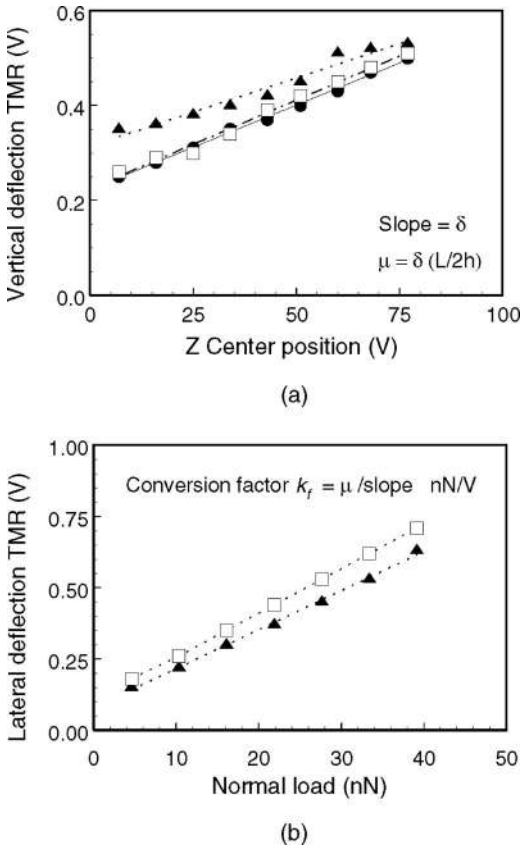

FIG. 4. Friction calibration data obtained on Al_2O_3 sample. (a) Three data sets of Trace minus Retrace (TMR) value of surface height as a function of normal load. The slope of this plot δ, is related to the coefficient of friction μ between sample and tip (Ref. 21). (b) Two data sets of TMR of lateral deflection signal as a function of normal load. Equating the slope of this plot to μ obtained from (a), the conversion factor to convert lateral deflection signal to friction force can be obtained (Ref. 21).

used for the calibration result in an elastic contact (no ploughing). Once the coefficient of friction is determined, contact mode scans perpendicular to the long axis of the cantilever beam are performed for various normal loads. The lateral deflection signals obtained are plotted as a function of normal load as shown in Fig. 4(b). By equating the slope of this plot to the previously obtained coefficient of friction (μ), a conversion factor k_f (in N/V) of the cantilever can be obtained, which can be used to convert the lateral deflection signal to force units. The value obtained for the conversion factor k_f using the above-mentioned method was 2.1 nN/V.

The above-used method assumes that the lateral forces acting on the tip act at the end of the tip. However in the experiment to measure the static friction force of the rotor, this is not the case. As seen in Fig. 3(b), a distance of 100–200 nm is maintained between the end of the tip and the top surface of the rotor. This results in the point of contact being 100–200 nm above the end of the tip (compared to a tip height of 5 μm). By performing a moment balance about the top of the tip for a force acting 200 nm above the end of the tip and an equivalent force acting at the end of the tip, we find that the actual force is about 2%–4% greater than an equivalent force acting at the end of the tip for a given deflection signal. This difference can be considered to be negligible and hence the conversion factor k_f can be used for the static friction force experiments. In addition the fact that the normal deflection signal does not change significantly [Fig. 3(d)] also validates the assumption that the tip undergoes torsion of the cantilever similar to the case when the force acts at the end of the tip. The static friction force can therefore be calculated from Eq. (2), as follows:

$$F_s = k_f V_f \frac{l_2}{l_1}, \tag{4}$$

where the distance l_1 is determined from Fig. 1 to be about 22 μm. The distance l_2 is maintained to be about 35 ± 5 μm during the experiments. This was achieved with the aid of the high-magnification camera equipped with the AFM. The variations in l_2 result in a variation of 25% in the calculated value of F_s using this technique.

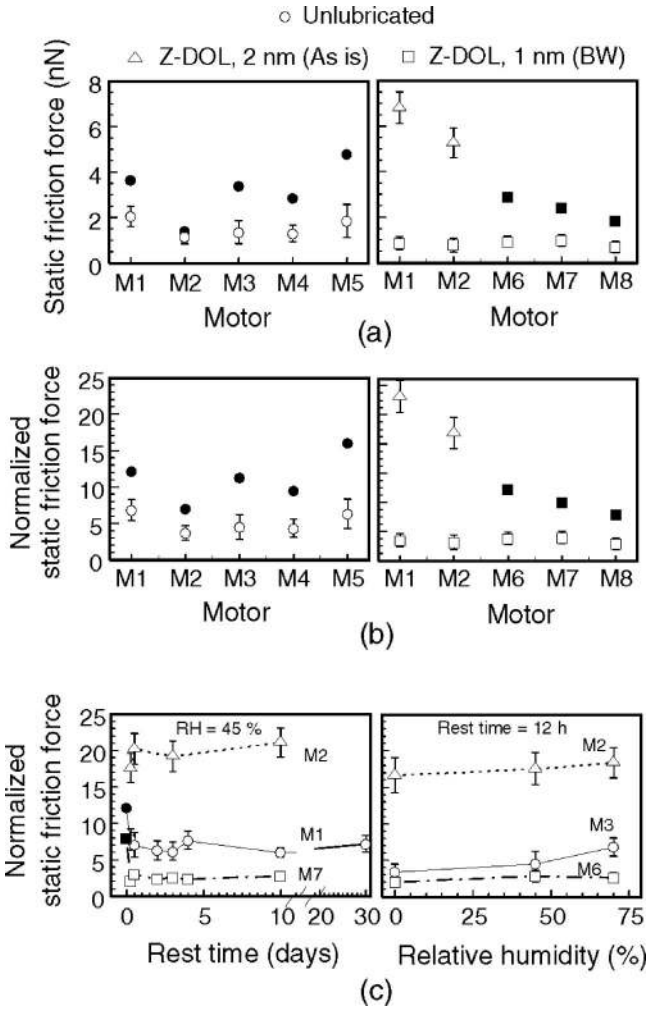

FIG. 5. (a) Static friction force data (raw and normalized with the weight of the rotor) for unlubricated and lubricated micromotors. The closed points indicate the force obtained in the first experiment for a given rotor, while the open points indicate values obtained on subsequent runs. Motors M1–M4 and M6–M8 are from batch 1 and M5 is from the batch 2. (b) Normalized static friction force data for selected micromotors as a function of rest time and relative humidity. Rest time is defined as the time elapsed between a given experiment and the first experiment in which motor movement was recorded (time 0). The motors were allowed to sit at a particular humidity for 12 h prior to measurements.

III. RESULTS

A. Static friction force measurements

Static friction force measurements were performed on five unlubricated micromotors (M1–M5). After static friction force experiments, two of the unlubricated motors (M1 and M2) were lubricated with a 2 nm-thick coating of Z-DOL (as-is). Three different motors (M6–M8) were directly lubricated with a 1 nm-thick bonded layer of Z-DOL before conducting experiments on them. Figure 5(a) presents the measured values of static friction force [as per Eq. (4)] for various unlubricated and lubricated micromotors. The closed symbols represent the static friction force measured on the very first experiment on a given motor. The open symbols represent values from subsequent experiments. Each open data point shown is an average of six measurements. The distribution of the data points was random. Figure 5(b) shows normalized static friction force, which is obtained by dividing the measured value of static friction force by the weight of the rotors, which was calculated to be 0.254 nN. Electrostatic and meniscus forces are not included here in the normal force, which would result in the value of coefficient of static friction lower than the values of the normalized static friction force reported here.

Figure 5(a) shows that in all cases, the initial static friction force is the highest for a given rotor. Subsequent values, although exhibiting considerable variability, are substantially lower. The initial values of static friction force (closed symbols) for unlubricated and lubricated are comparable to each other, with normalized values being between 5 and 12, which are slightly higher than the values in Table II for polysilicon/polysilicon. However the effect of the bonded lubricant layer

TABLE II. Surface roughness parameters and microscale coefficient of friction for various micromotor component surfaces measured using an AFM. Mean and $\pm 1\sigma$ values are given.

	rms roughness[a] (nm)		Peak-to-valley distance[a] (nm)		Skewness[a] Sk		Kurtosis[a] K		Microscale coefficient of friction[b] (μm)	
	1[c]	2[c]	1	2	1	2	1	2	1	2
Rotor topside	21 ± 0.6	20 ± 1	225 ± 23	210 ± 26	1.4 ± 0.30	0.90 ± 0.11	6.1 ± 1.7	5.3 ± 1.4	0.07 ± 0.02	0.08 ± 0.01
Rotor underside	14 ± 2.4	⋯	80 ± 11	⋯	-1.0 ± 0.22	⋯	3.5 ± 0.50	⋯	0.11 ± 0.03	⋯
Stator topside	19 ± 1	21 ± 0.7	246 ± 21	150 ± 10	1.4 ± 0.50	1.1 ± 0.10	6.6 ± 1.5	3.9 ± 0.30	0.08 ± 0.01	0.08 ± 0.01

[a]Measured from a tapping mode AFM scan of size 5 μm×5 μm using a standard Si tip scanning at 5 μm/s in a direction orthogonal to the long axis of the cantilever.
[b]Measured using an AFM in contact mode at 5 μm×5 μm scan size using a standard Si_3N_4 tip scanning at 10 μm/s in a direction parallel to the long axis of the cantilever.
[c]1 and 2 correspond to batches 1 (M1–M4, M6–M8) and 2 (M5).

can be seen in the subsequent measurements. The values of normalized static friction force for M6–M8 are a little lower (under 4) than that of the unlubricated motors and also show much less variability. A layer of as-is mobile lubricant produces disastrously high values of static friction force that are up to 3 to 5 times higher than that of unlubricated motors (M1 and M2). Upon subsequent bonding and washing, M1 and M2 show static friction forces comparable to M6–M8 that appear to be lower than the unlubricated case. Thus a bonded layer of Z-DOL appears to result in some improvement in the static friction characteristics of the motors, while even a 2-nm-thick mobile layer results in very high friction forces.

B. Effect of rest time and humidity

Figure 5(c) shows the normalized static friction forces for unlubricated and lubricated motors as a function of rest time. Rest time here is defined as the time elapsed between the first experiment conducted on a given motor (closed symbol at time zero) and subsequent experiments (open symbols). Each open symbol data point is an average of six measurements. It can be seen that for the unlubricated motor (M1) and the motor lubricated with a bonded layer of Z-DOL (M7), the static friction force is highest for the first experiment and then drops to an almost constant level. In the case of the motor with an as-is mobile layer of Z-DOL, the values remain very high up to 10 days after lubrication.

In order to study the effect of humidity on the static friction forces of the micromotors, the samples were housed for 12 h at a given humidity in a control chamber with separate inlets for dry and humid air. The humidity was maintained to $\pm 3\%$ RH except for 0% which showed no variation. The sample was then taken out of the chamber and the static friction test was performed using the AFM, usually within 15 min. Figure 5(c) also shows normalized static friction forces on unlubricated and lubricated motors as a function of relative humidity. In all cases, there is negligible difference in the static friction force at 0% and 45% RH. This is probably due to the fact that the motors were stored in ambient (45% RH) for some period of time before the humidity tests and a 12 h period of confinement at 0% RH would probably not eliminate all the water films on the sample surface. At 70% RH, the unlubricated motor (M3) exhibits a substantial increase in the static friction force, while the motor with bonded Z-DOL (M6) shows no increase in static friction force due to the hydrophobicity of the lubricant layer. The motor with an as-is mobile layer of the lubricant (M2) shows consistently high values of static friction force that varies little with humidity.

C. Surface roughness measurements

Most of the friction forces resisting motion in the micromotor are concentrated near the rotor–hub interface where continuous physical contact occurs. Surface roughness of the surfaces usually has a strong influence on the friction characteristics on the micro/nanoscale. Table II shows various surface roughness parameters obtained from 5 μm scans of the various component surfaces of several unlubricated micromotors using the AFM in tapping mode. A surface with a Gaussian height distribution should have a skewness of zero and kurtosis of three.[22] Although the rotor and stator top surfaces exhibit comparable roughness parameters, the underside of the rotors exhibits lower rms roughness and peak-to-valley values. More importantly, the rotor underside shows negative skewness and lower kurtosis than the topsides, both of which are conducive to high real area of contact[22] and hence high friction. The rotor underside also exhibits higher microscale coefficient of friction than the rotor topside and stator. Surfaces for batch 1 show higher P-V, skewness, and kurtosis values as compared to batch 2. The increased roughness is desirable for low friction. It was reported that batch 1 motors ran after lubrication whereas motors of batch 2 did not.[23]

Figure 6 shows representative surface height maps of the various surfaces of a micromotor measured using the AFM in tapping mode. The rotor underside exhibits varying topography from the outer edge to the middle and inner edge. At the outer edges, the topography shows smaller circular asperities, similar to the topside. The middle and inner regions show deep pits with fine edges that may have been created by the first etching step (see Fig. 2). Previous studies have also shown that etching can affect the surface roughness of

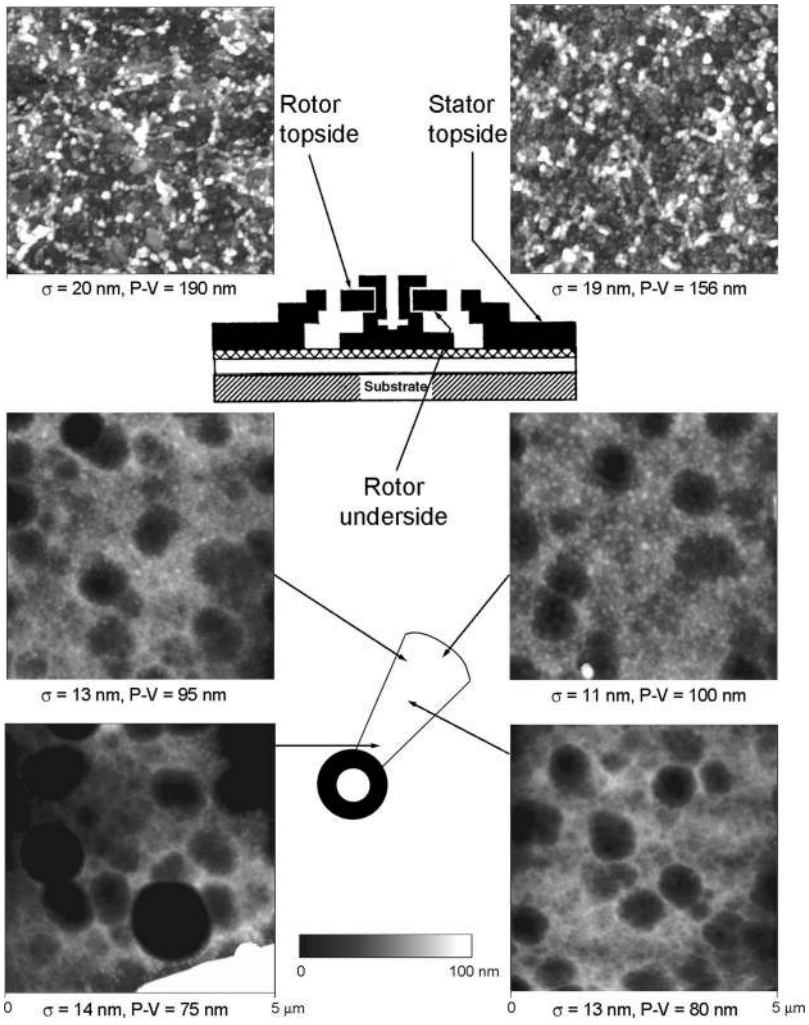

FIG. 6. Representative AFM surface height images obtained in tapping mode (5 μm×5 μm scan size) of various component surfaces of the micromotors (Images shown are that of motor M1). rms roughness (σ) and peak-to-valley *(P–V)* values of the surfaces are given. The underside of the rotor exhibits drastically different topography from the topside.

surfaces in surface micromachining.[9] Figure 7 shows surface roughness of the surface beneath the rotors (the first polysilicon layer). There appears to be a difference in the roughness between the portion of this surface that was initially underneath the rotor (region B) during fabrication (right) and the portion that was away from the rotor and hence always exposed (region A). The former region shows lower roughness than the latter region. This suggests that the surfaces at the rotor–hub interface that come into contact at the end of the fabrication process exhibit large real areas of contact that result in high friction.

IV. DISCUSSION

Figure 8 summarizes static friction force data for motors M1 and M2 along with schematics of the meniscus effects for the unlubricated and lubricated surfaces. Capillary condensation of water vapor from the environment results in formation of meniscus bridges between contacting and near-contacting asperities of two surfaces in close proximity to each other as shown in Fig. 8. For unlubricated surfaces, more menisci are formed at higher humidity resulting in higher friction force between the surfaces.[24] The formation of meniscus forces is supported by the fact that the static friction force for unlubricated motors increases at high humidity [Fig. 5(c)]. Solid bridging may occur near the rotor-hub interface due to silica residues after the first etching process.[9] In addition the drying process after the final etch can result in liquid bridging formed by the drying liquid due to capillary force at these areas.[4,8,9,22] The initial static friction force therefore will be quite high as evidenced by the closed data points in Fig. 5. Once the first movement of the rotor permanently breaks these solid and liquid bridges, the static friction force of the motors will drop (as seen in Fig. 5) to a value dictated predominantly by the adhesive energies of rotor and hub surfaces, the real area of contact between these surfaces and meniscus forces due to water vapor in the air, at which point the effect of lubricant films can be observed.

Lubrication with a mobile layer, even a thin one, results in very high static friction forces due to meniscus effects of the lubricant liquid itself at and near the contact regions. It should be noted that a motor submerged in a liquid lubricant would result in a fully flooded lubrication regime.[22] In this case there is no meniscus contribution and only the viscous contribution to the friction forces would be relevant. A motor submerged in silicon oil did run.[23] However, this may not be a practical method of lubricating motors. A solidlike hydro-

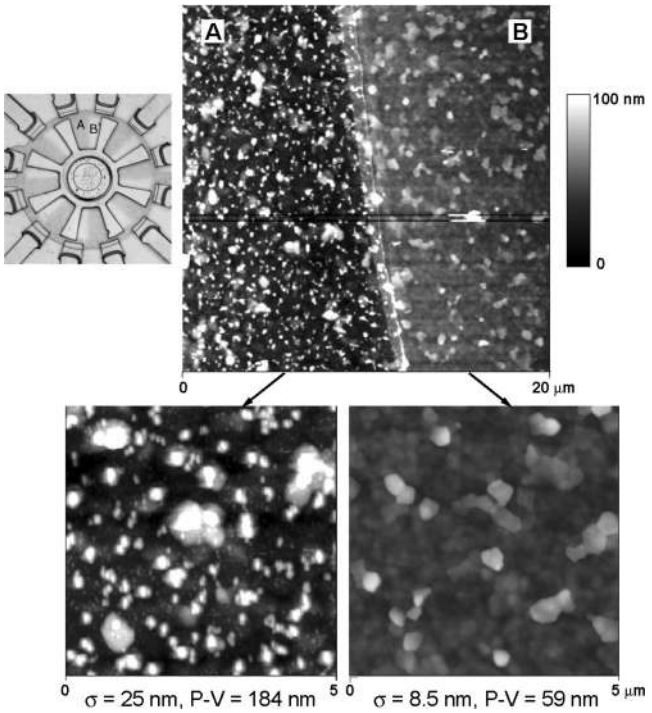

FIG. 7. Surface height images of polysilicon regions directly below the rotor (for motor M1). Region A is away from the rotor while region B was initially covered by the rotor prior to the release etch of the rotor. During this step, slight rotation of the rotor caused region B to be exposed.

phobic lubricant layer (such as bonded Z-DOL) results in favorable friction characteristics of the motor. The hydrophobic nature of the lubricant inhibits meniscus formation between the contact surfaces and maintains low friction even at high humidity [Fig. 5(c)]. This suggests that solidlike hydrophobic lubricants are ideal for lubrication of MEMS while mobile lubricants result in increased values of static friction force.

V. CONCLUSIONS

A novel technique to measure the static friction force of surface micromachined polysilicon micromotors using an AFM was described. Static friction forces normalized to the rotor weight for a Polysilicon–polysilicon contact were found to be in the range of 4–10 for unlubricated micromotors. A bonded layer of Z-DOL appeared to provide good lubrication to the micromotors by reducing the normalized static friction force to below 4. A thin mobile layer of lubricant resulted in static friction forces up to three times higher than the values obtained for unlubricated ones. A variation in the static friction forces with humidity was observed for the unlubricated motors, which was explained in terms of meniscus effects at the rotor–hub interface. The undersides of the rotors exhibit drastically different topography from the topsides due to contact with etchants and favor large real areas of contact and high friction forces. Solidlike hydrophobic lubricants appear to be ideal for lubrication of MEMS.

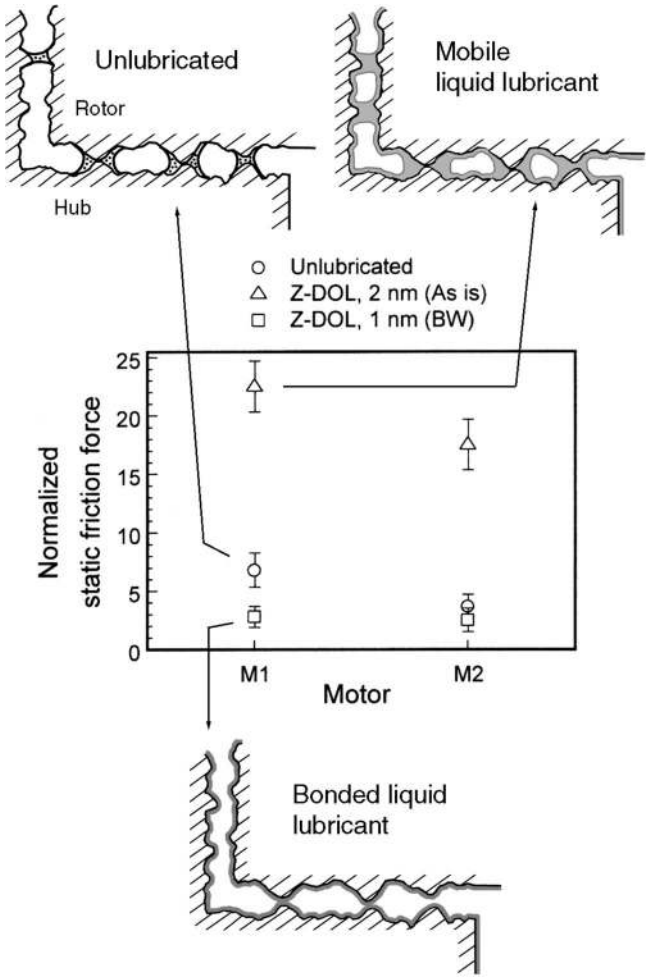

FIG. 8. Summary of effect of liquid and solid lubricants on static friction force of micromotors. Despite the hydrophobicity of the lubricant used (Z-DOL), a mobile liquid lubricant (Z-DOL as-is) leads to very high static friction force due to increased meniscus forces whereas a solidlike lubricant (bonded Z-DOL) appears to provide some amount of reduction in static friction force.

ACKNOWLEDGMENTS

The micromotors used in the study (M1–M8) were obtained from Dr. N. Fabre and V. Conedera during their visit to our laboratory from LAAS-CNRS, Toulouse France. We are extremely grateful to them and to Dr. H. Camon, LAAS-CNRS, for their discussions regarding the fabrication processes and for their insights into the friction problems associated with the motors. We thank Dr. Z. Zhao and Dr. H. Liu of CMCL for their help in lubricating the motors. Financial support for this research was provided by the National Science Foundation (Contract No. ECS-9820022). The content of this information does not necessarily reflect the position or policy of the Government and no official endorsement should be inferred.

[1]*Micromachines and MEMS, Classic and Seminal Papers to 1990,* edited by W. Trimmer (IEEE Press, New York, 1997).
[2]M. Madou, *Fundamentals of Microfabrication* (Chemical Rubber Corp., Boca Raton, FL, 1997).

[3]*Tribology Issues and Opportunities in MEMS,* edited by B. Bhushan (Kluwer, Dordrecht, 1998).
[4]B. Bhushan, in *Handbook of Micro/Nanotribology,* 2nd ed., edited by B. Bhushan (Chemical Rubber Corp., Boca Raton, FL, 1999), pp. 797–831.
[5]B. Bhushan, *Tribology and Mechanics of Magnetic Storage Devices,* 2nd ed. (Springer, New York, 1996).
[6]H. Guckel and D. W. Burns, Sens. Actuators **20**, 117 (1989).
[7]T. Abe, W. C. Messner, and M. L. Reed, J. Microelectromech. Syst. **4**, 66 (1995).
[8]C. H. Mastrangelo and C. H. Hsu, J. Microelectromech. Syst. **2**, 33 (1993).
[9]R. Maboudian and R. T. Howe, J. Vac. Sci. Technol. B **15**, 1 (1997).
[10]Y. C. Tai and R. S. Muller, Sens. Actuators A **A21-A23**, 180 (1990).
[11]M. G. Lim, J. C. Chang, D. P. Schultz, R. T. Howe, and R. McV. White, Proceedings of the IEEE Third MEMS Workshop, Napa Valley, CA, February 1990, pp. 82–88.
[12]R. Maboudian, MRS Bull. **23** , 47 (1998).
[13]D. Matheison, U. Beerschwinger, S. J. Young, R. L. Rueben, M. Taghizadeh, S. Eckert, and U. Wallrabe, Wear **192**, 199 (1996).
[14]In Ref. 4, p. 7.
[15]K. Deng, R. J. Collins, M. Mehregany, and C. N. Sukenik, Proceedings of the MEMS 95, Amsterdam, Netherlands, January–February, 1995.
[16]B. Bhushan, A. V. Kulkarni, V. N. Koinkar, M. Boehm, L. Odoni, C. Martelet, and M. Belin, Langmuir **11**, 3189 (1995).
[17]U. Srinivasan, M. R. Houston, R. T. Howe, and R. Maboudian, J. Microelectromech. Syst. **7**, 252 (1998).
[18]V. Conedera, N. Fabre, H. Camon, B. Rousset, H. H. Pham, and C. Solano, Sens. Actuators A **46-47**, 82 (1995).
[19]Z. Zhao and B. Bhushan, Wear **202**, 50 (1996).
[20]*Nanoscope Command Reference Manual, Version 4.22ce,* Digital Instruments, 1996.
[21]J. Ruan and B. Bhushan, ASME J. Tribol. **116**, 378 (1994).
[22]B. Bhushan, *Principles and Applications of Tribology* (Wiley, New York, 1999).
[23]H. Camon, LAAS-CNRS, Toulouse, France (private communications).
[24]B. Bhushan and S. Sundararajan, Acta Mater. **46**, 3793 (1998).